Kırklareli Üniversitesi
Mühendislik ve Fen Bilimleri Dergisi
Cilt 10, Sayı 2, 246-255, 2024

Kırklareli University
Journal of Engineering and Science
Volume 10, Issue 2, 246-255, 2024

Research Article DOI: 10.34186/klujes.1565394

Diode and Photodetector Characterization of Van der Waals Type InSe/CdS Heterojunction Device

Fatih Ünal[1*]

[1]*Giresun University, Central Research Laboratory Application and Research Center, Giresun, Türkiye,*

Received: 11.10.2024, Accepted: 12.12.2024, Published: 25.12.2024

ABSTRACT

In this study, an InSe thin film layer was deposited onto a CdS thin film layer produced via the chemical bath deposition (CBD) method using the Successive Ionic Layer Adsorption and Reaction (SILAR) technique. The produced heterojunction devices were divided into two groups, and one group was annealed in an ambient atmosphere at 80°C for 1 hour. The electrical characterization of both heterojunction devices was performed in the dark and under an illumination intensity of 100 mW/cm². The fundamental diode parameters (n, ϕ_b, Rs, I_0) were analyzed using different methods. In the dark environment, these values are 8.47, 0.94 eV, 2.27×10^8 Ω and 2.12×10^{-11} A for In/InSe/In and 8.43, 0.96 eV, 7.27×10^8 Ω ve 7.07×10^{-12} A for In/$InSe_{annealed}$/In, respectively. Furthermore, key photodetector parameters such as photocurrent, photoresponsivity, photosensitivity, and specific detectivity were determined for these two devices.

Keywords: InSe; CdS; Photodetector.

Van der Waals tipi InSe/CdS Heteroeklem Cihazının Diyot ve Fotodedektör Karakterizasyonu

ÖZ

Bu çalışmada kimyasal banyo depolama (CBD) yöntemiyle üretilen CdS ince film tabakasının üzerine InSe ince film tabakası Sıralı İyonik Tabaka Adsorpsiyon ve Reaksiyon (SILAR) yöntemiyle biriktirilmiştir. Üretilen heteroeklem cihazları iki gruba ayrılmış ve bir grup atmosfer ortamında 80 ºC sıcaklıkta 1 saat tavlanmıştır. Her iki heteroeklem cihazının elektriksel karakterizasyon karanlık ve 100 mW/cm² ışık şiddetinde gerçekleştirilmiştir. Temel diyot parametreleri (n, ϕ_b, Rs, I_0) farklı yöntemlerle analiz edilmiştir. Karanlık ortamda sırasıyla bu değerler In/InSe/In için 8.47, 0.94 eV, 2.27×10^8 Ω ve 2.12×10^{-11} A iken In/$InSe_{annealed}$/In için 8.43, 0.96 eV, 7.27×10^8 Ω ve 7.07×10^{-12} A'dir. Bu iki cihazın temel fotodedektör parametreleri olan fotoakım, fotoduyarlılık, fotohassasiyet ve özgün algılama değerleri belirlenmiştir.

Anahtar Kelimeler: InSe; CdS; Fotodedektör.

*Corresponding Author: *Fatih Ünal*
fatih.unal@giresun.edu.tr

1. INTRODUCTION

Wide photodetectors covering the visible, ultraviolet, and near-infrared electromagnetic spectrum are now used in a variety of applications, including aircraft, night vision medical imaging, solar cells, broad spectral switches, light communications, and biometric identification (Chen et al., 2017; Hu et al., 2014; Yan et al., 2022). The introduction of graphene has significantly transformed the van der Waals layered material family(Novoselov et al., 2004). This has also led to the development of photodetectors based on layered materials that have extremely high sensitivity. Properties such as atomic-level thickness and facile electrical structure adjustment by external forces (Wang et al., 2017) offer substantial potential for the development of nanoscale photodetectors (Islam et al., 2019). III-VI binary semiconductors have sparked intense research interest in recent years due to their intriguing electrical and optical characteristics, as well as potential applications in electronic and optoelectronic devices. Several high-performance devices, including solar cells, photodetectors, and transistors, have been reported (Chen et al., 2017; Huang et al., 2011). Among these semiconductors, indium selenide (InSe) is an essential layered semiconductor with a high direct bandgap and effective visible light absorption. These qualities make it a viable contender for a wide range of essential applications, including solar energy conversion, random access memory, photodetectors, and visible optoelectronics (Yadav & Salunke, 2015; Zhai et al., 2010). Cadmium sulfide (CdS), a member of the II-VI group, is a widely used compound in optoelectronic devices. It stands out due to its low resistivity, high transmittance in the visible region, and good electron affinity (Diso, Fauzi, Echendu, Weerasinghe, & Dharmadasa, 2011; Kumarage, Wijesundera, Seneviratne, Jayalath, & Dassanayake, 2017; Lade & Lokhande, 1997). CdS thin films are considered one of the most exciting options for heterojunction thin film photodetectors, solar cell etc.(Ashour, 2003). In this study, we combined CdS and InSe compounds in the form of a van der Waals heterojunction and investigated the diode and photodetector parameters.

2. EXPERIMENTAL DETAILS

The InSe thin film was previously deposited onto a CdS layer, approximately 100 nm thick, prepared by the chemical bath deposition method using the Successive Ionic Layer Adsorption and Reaction (SILAR) technique. The precursor solutions were 0.07 M $In_2(SO_4)_3$ and 0.05 M Na_2SeSO_3. In each cycle, a layer approximately 1.5 nm thick was formed, and the total number of cycles was 45. The total thickness of the InSe thin film was approximately 70 nm. The details of the procedure have been presented in our previous studies (Ünal, 2013, 2021). The fabricated InSe/CdS heterojunctions were divided into two groups, with one group annealed at 80°C for 1 hour in an ambient atmosphere. Subsequently, In (indium) metal contacts were applied to the InSe layer. Figure 1 presents the production mechanism and a schematic representation

of the layers. The I-V measurements were performed using a Keithley 6486 picoammeter and Pasco Scientific SF-9585.

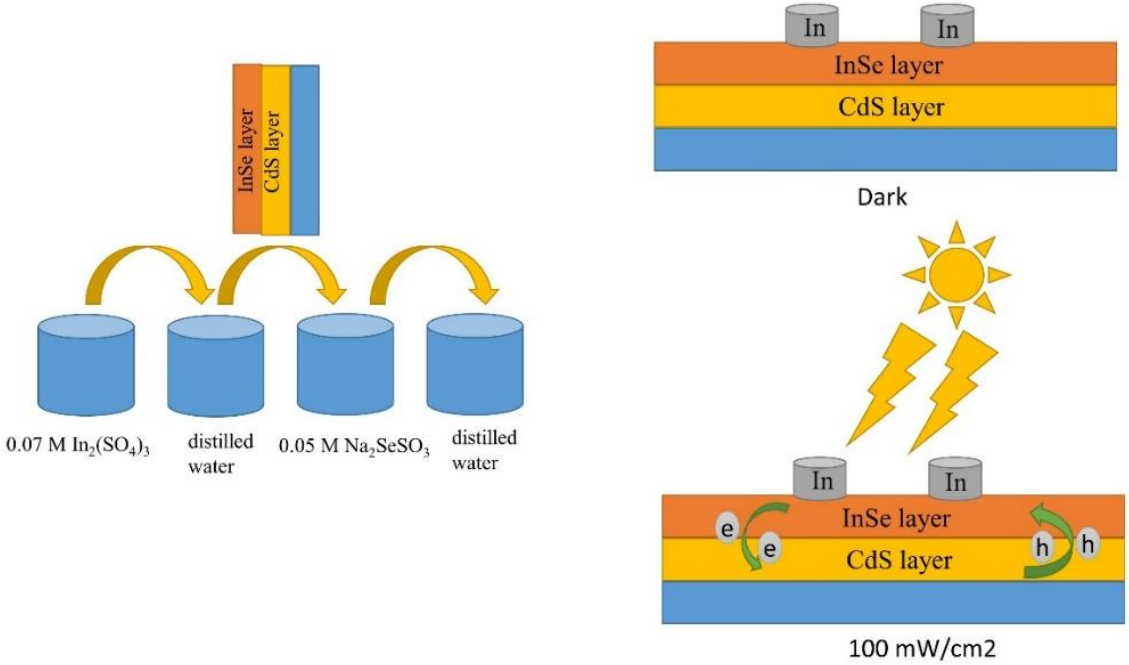

Figure 1: The production mechanism and schematic representation of the heterojunctions.

3. RESULT AND DISCUSSION

The basic electrical characterization of the In/InSe/In and In/$InSe_{annealed}$/In devices was determined using current-voltage (I-V) curves. The I-V characterization of the devices, fabricated with both annealed and unannealed InSe grown on CdS, was examined under forward bias at an applied potential range of 0-20 V at room temperature, in the dark, and under an illumination intensity of 100 mW/cm². The I-V curves of these devices, measured under dark conditions and at an illumination intensity of 100 mW/cm², are presented in Figure 2a. In all four curves, the current increased linearly up to approximately 0.5 V, after which this increase diminished due to the influence of series resistance. It is clearly observed that the current values increased with illumination intensity in both devices.

Based on the I-V curve and using different methods, the fundamental electrical parameters of the designed devices, such as diode ideality factor (n), barrier height (ϕ_b), reverse saturation current (I_0), series resistance (Rs), and others, can be determined. The most commonly used methods for this purpose include thermionic emission theory, the modified Norde method, and Cheung & Cheung functions (Cheung & Cheung, 1986; Norde, 1979; Racko, Grmanová, & Breza, 1996).

Thermionic emission theory (TE) is one of the most commonly used methods, and the link between current and voltage is given in Equation 1,

$$I = I_0 \exp\left(\frac{q(V-IR_s)}{nkT}\right)[1 - \exp\left(\frac{-q(V-IR_s)}{kT}\right)] \quad (1)$$

where q, k, and T represent the electrical charge, Boltzmann constant, and temperature, respectively. Ideal diodes have n values of 1 and I_0 is determined using the line intercept of lnI at $V = 0$, as shown in Equation 2,

$$I_0 = AA^*T^2 \exp\left(-\frac{q\phi_b}{kT}\right) \quad (2)$$

To compute n and ϕ_b, rearrange the equations above and use the slope and cut point in the linear zone of the graph of $\ln I - V$, as shown in Equations 3 and 4, respectively.

$$n = \frac{q}{kT}\frac{dV}{d(\ln(I))} \quad (3)$$

$$\phi_b = \frac{kT}{q}\ln\frac{AA^*T^2}{I_0} \quad (4)$$

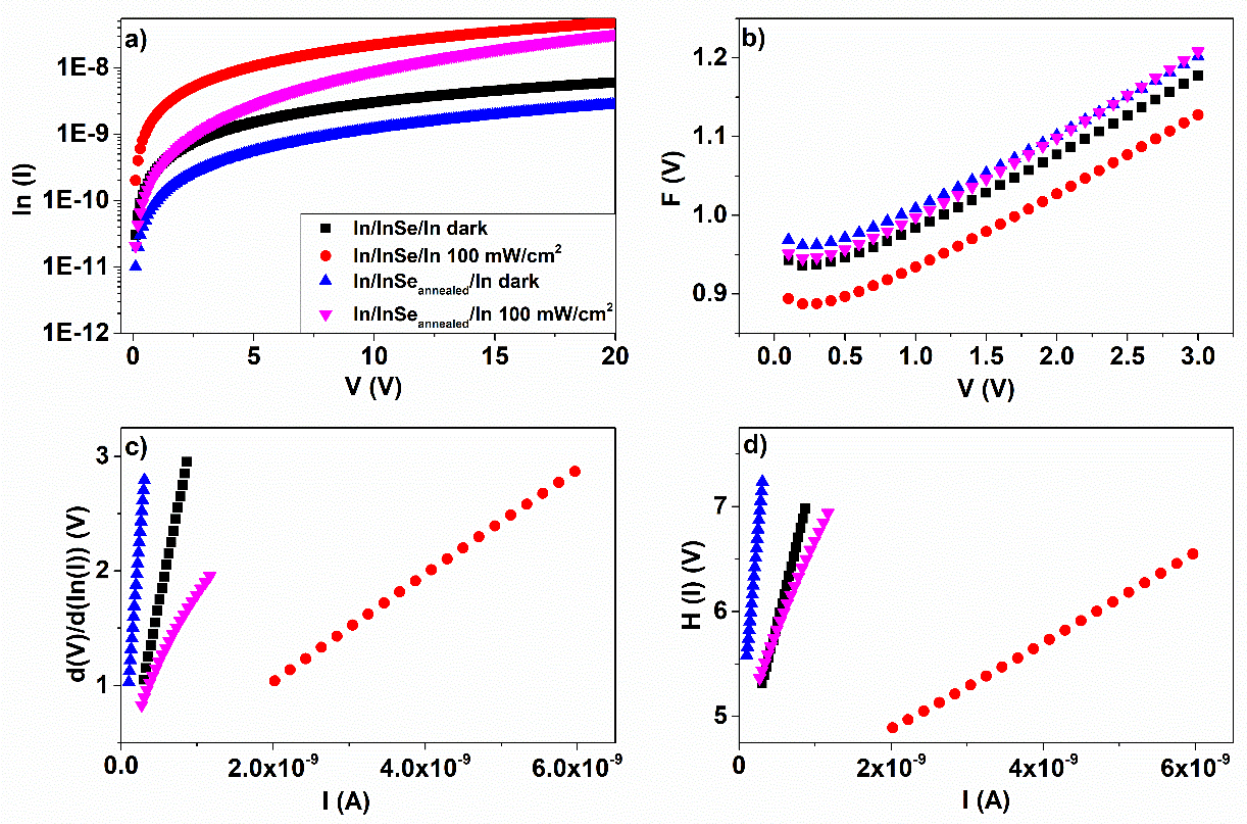

Figure 2: The In/InSe/In and In/InSe$_{annealed}$/In devices under dark conditions and at 100 mW/cm² illumination intensity: a) I-V characterization, b) the variation of the F(V) function with respect to V, c) the variation of the d(V)/d(ln(I)) function with respect to I, and d) the variation of the H(I) function with respect to I.

The values of the *n* determined from thermionic emission (TE) for In/InSe/In and In/$InSe_{annealed}$/In devices under dark conditions are 8.47 and 8.43, respectively, whereas under an illumination intensity of 100 mW/cm², the *n* values for In/InSe/In and In/$InSe_{annealed}$/In devices are 8.45 and 7.91, respectively. ϕ_b values determined from TE under dark conditions for In/InSe/In and In/$InSe_{annealed}$/In devices are 0.94 eV and 0.96 eV, respectively, while under 100 mW/cm² illumination, the $\phi_b$values for these devices are 0.89 eV and 0.94 eV, respectively. I_o values determined under dark conditions for In/InSe/In and In/$InSe_{annealed}$/In devices are $2.12x10^{-11}$ A and $7.07x10^{-12}$ A, respectively, while under 100 mW/cm² illumination, the I_o values for these devices are $1.41x10^{-10}$ A and $1.42x10^{-11}$ A, respectively.

The decrease in *n* and $\phi_b$values calculated by TE under illumination, along with the increase in I_o, is an expected behavior. Additionally, the decrease in the n value after annealing brings the device closer to ideality. However, the determined values remain far from the ideal value of 1. There could be several reasons for this, which are commonly encountered in the literature (Coşkun, Ünal, & Koç, 2023; İlhan, Gorunmez Gungor, Koc, Coşkun, & Yakuphanoğlu, 2023; Koç et al., 2024) . These include barrier inhomogeneities, the influence of series resistance, the formation of unwanted oxide layers, recombination at the interface, and the occurrence of contamination during the experimental process (Güllü, Aydoğan, & Türüt, 2012; Unal et al., 2024).

The modified Norde technique is a typical method for finding the ϕ_b and *Rs* as indicated by equation 5.

$$F(V) = \frac{V}{\gamma} - \frac{kT}{q} - \ln(\frac{I(V)}{A.A^*T^2}) \tag{5}$$

where *I(V)* is the current acquired from the *I-V* experiment. *γ* is a dimensionless arbitrary integer computed from the *I-V* curve with a value higher than the ideality factor. Additionally. ϕ_b is determined using the information supplied below.

$$\phi_b = F(V_0) + \frac{V_0}{\gamma} - \frac{kT}{q} \tag{6}$$

$F(V_0)$ is the maximal point of *F(V)*, whereas V_0 represents the voltage at that moment. Furthermore, *Rs* values derived from Norde functions are supplied by the following equation:

$$R_s = \frac{kT(\gamma - n)}{qI_0} \tag{7}$$

where, I_0 is the lowest current corresponding to the lowest current in *F(V)*.

In Figure 2b, the variation curve of the *F(V)* function against *V* is presented. ϕ_b values for In/InSe/In and In/InSe$_{annealed}$/In devices, determined from the modified Norde method under dark conditions, are 0.93 eV and 0.95 eV, respectively. Under an illumination intensity of 100 mW/cm², the ϕ_b values determined for In/InSe/In and In/InSe$_{annealed}$/In devices using the modified Norde method are 0.88 eV and 0.94 eV, respectively. *Rs* values for In/InSe/In and In/InSe$_{annealed}$/In devices determined from the modified Norde method under dark conditions are 2.27 x 10^8 Ω and 7.27 x 10^8 Ω, respectively, while under an illumination intensity of 100 mW/cm², the *Rs* values are 3.42 x 10^7 Ω and 5.21 x 10^7 Ω, respectively.

In the Cheung and Cheung method, *n*, ϕ_b, and *Rs* values of the diode are determined using the Cheung and Cheung functions (Cheung & Cheung, 1986). The Cheung and Cheung functions are provided in Equations 8, 9, and 10.

$$\frac{dV}{dln(I)} = IR_s + \frac{nkT}{q} \tag{8}$$

$$H(I) = V - \frac{nkT}{q}\ln(\frac{I}{AA^*T^2}) \tag{9}$$

$$H(I) = IR_s + n\emptyset_b \tag{10}$$

In the above equations, starting from the region where the curve bends in the *ln(I)-V* graph, the graphs of *dV/dln(I)* and *H(I)* as functions of *I* are plotted. The slope of the *dV/dln(I)* vs. *I* graph gives the *Rs* while n is calculated from the y-intercept of the curve using other constants. In the *H(I)* vs. *I* graph, the $\emptyset_b$ is determined from the y-intercept using the *n* value, and the slope of this curve gives the *Rs*.

Figure 2c presents the variation of *d(V)/d(ln(I))* as a function of *I*. The *n* values determined from the *d(V)/d(ln(I))* vs. *I* graph under dark conditions for the In/InSe/In and In/InSe$_{annealed}$/In devices are 1.86 and 6.05, respectively, while under 100 mW/cm² illumination, the *n* values are 4.37 and 21.81, respectively. The *Rs* values determined from the *d(V)/d(ln(I))* vs. *I* graph under dark conditions for the In/InSe/In and In/InSe$_{annealed}$/In devices are 3.33x10^9 Ω and 8.61x10^9 Ω, respectively, while under 100 mW/cm² illumination, the *Rs* values are 4.63x10^8 Ω and 1.24x10^9 Ω, respectively.

Figure 2d shows the variation of *H(I)* as a function of *I*. The $\emptyset_b$ values determined from the *H(I)* vs. *I* graph under dark conditions for the In/InSe/In and In/InSe$_{annealed}$/In devices are 2.37 eV and 0.72 eV, respectively, while under 100 mW/cm² illumination, the $\emptyset_b$values are 0.91 eV and 0.22 eV, respectively. The *Rs* values determined from the *H(I)* vs. *I* graph under dark conditions for the In/InSe/In and In/InSe$_{annealed}$/In devices are 2.93x10^9 Ω and 8.11x10^9 Ω, respectively, while under 100 mW/cm² illumination, the *Rs* values are 4.21x10^8 Ω and 1.75x10^9 Ω, respectively.

While there is consistency in the values of $\emptyset_b$ and *Rs* calculated using different methods, no such consistency is observed for the n values. The *n* values determined via thermionic emission (TE) use the linear region of the *I-V* curve, whereas the Cheung & Cheung functions perform their calculations in the region where the linearity of the *I-V* curve starts to deviate. This difference in the regions of the *I-V* curve being used leads to discrepancies in the *n* values.

Figure 3 shows the variation of the photodetector parameters of the In/InSe/In and In/$InSe_{annealed}$/In devices under an applied potential of 0-20 V. In Figure 3a, the photocurrent ($I_{ph} = I_{ill} - I_{dark}$) (Demirezen et al., 2022; Ünal, 2022) variations of the devices are presented, where I_{ill} is the current under illumination, and I_{dark} is the current in dark conditions. For both devices, the I_{ph} values increased with rising applied voltage. The maximum I_{ph}values were observed at 20 V, with maximum I_{ph}values of 4.2x10^{-8} A for the In/InSe/In and 2.92x10^{-8} A for the In/$InSe_{annealed}$/In device. In all regions, the I_{ph}values for the In/InSe/In device were higher than those for the In/$InSe_{annealed}$/In device.

Figure 3b shows the photoresponsivity ($R= I_{ph}/PA$) (Demirezen et al., 2022; Kurt, Aktas, Ünal, & Kabaer, 2022) values of the devices, where I_{ph} is the photocurrent, *P* is the incident light power, and *A* is the active area. In Figure 3b, while the *R* values of the In/InSe/In device increased almost linearly, the *R* values of the In/$InSe_{annealed}$/In device increased exponentially and reached their maximum. For both devices, the maximum *R* values were observed at 20 V. The maximum *R* value was 2.8x10^{-5} A/W for the In/InSe/In device and 1.94x10^{-5} A/W for the In/$InSe_{annealed}$/In device.

Figure 3c presents the photosensitivity ($PS\% = 100\ x\ (I_{ph} - I_{dark})/I_{dark}$) (Aktas et al., 2023; Demirezen et al., 2022) values of the devices. Between 0 and 9.6 V of applied potential, the *PS%* values of the In/InSe/In device were higher, while between 9.6 and 20 V, the *PS%* values of the In/$InSe_{annealed}$/In device were higher. The maximum *PS%* values for both devices were observed at 20 V. The maximum *PS%* value was 8.02x10^{2} for the In/InSe/In device and 1.14x10^{3} for the In/$InSe_{annealed}$/In device.

Figure 3d shows the specific detectivity ($D^* = R\sqrt{A}\ /(2qI_{dark})^{1/2}$) (Unal et al., 2024; Zheng et al., 2016) values of the devices. For both devices, the *D** values exhibited a similar trend to the other parameters. The maximum *D** values were observed at 20 V. The maximum *D** value was 6.4x10^{8} Jones for the In/InSe/In device and 6.5x10^{8} Jones for the In/$InSe_{annealed}$/In device.

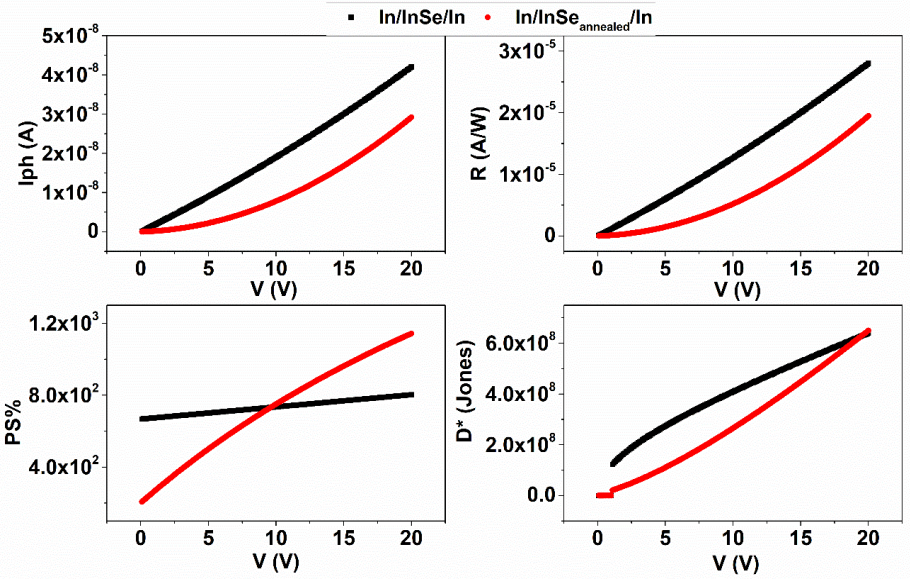

Figure 3: Variation of a) I_{ph}, b) *R*, c) *PS%*, and d) *D** values as a function of applied voltage for In/InSe/In and In/InSe$_{annealed}$/In devices under 100 mW/cm² illumination intensity.

4. CONCLUSION

In this study, InSe/CdS van der Waals type heterojunction devices were successfully fabricated using different chemical methods, with one group being annealed. The basic diode parameters of the fabricated heterojunction devices were determined and compared under dark conditions and 100 mW/cm² illumination intensity using different methods. According to the TE method, the *n* values decreased due to both the effect of annealing and light intensity. The Rs and ϕ_b values, determined through various methods, increased with annealing but decreased under illumination. Additionally, the fundamental photodetector parameters of the fabricated heterojunction devices were determined in the 0–20 V applied potential range. Based on these determinations, it was observed that the *Iph* and *R* values were higher in the In/InSe/In device, while the *PS%* and *D** values were higher in the In/InSe_annealed/In device at higher voltage regions.

CONFLICT OF INTEREST STATEMENT

There is no conflict of interest among the authors.

ACKNOWLEDGEMENT

This work was produced from the master's thesis titled "Growth of InSe thin films on different substrates and investigation of their optical, structural and photoelectric properties". I would like to thank Prof. Dr. Hasan Mammadova, who is not with us.

CONTRIBUTIONS OF AUTHORS

F.Ü.: Conceptualization, methodology, software, validation, formal analysis, investigation, resources, writing original draft preparation.

REFERENCES

Aktas, S., Unal, F., Kurt, M. S., Koç, M. M., Arslan, T., Aslan, N., & Coşkun, B. (2023). Investigation of fundamental electrical and optoelectronic properties of an organic- and carbon-based MnPc/GC photodiode with high photosensitivity. *Physica Scripta, 98*(9), 095504. doi:10.1088/1402-4896/aceb41

Ashour, A. (2003). Physical properties of spray pyrolysed CdS thin films. *Turkish Journal of Physics, 27*(6), 551-558.

Chen, S., Liu, X., Qiao, X., Wan, X., Shehzad, K., Zhang, X., . . . Fan, X. (2017). Facile synthesis of γ-In2Se3 nanoflowers toward high performance self-powered broadband γ-In2Se3/Si heterojunction photodiode. *Small, 13*(18), 1604033.

Cheung, S. K., & Cheung, N. W. (1986). Extraction of Schottky diode parameters from forward current-voltage characteristics. *Applied Physics Letters, 49*(2), 85-87. doi:10.1063/1.97359

Coşkun, B., Ünal, F., & KOÇ, M. M. (2023). Photodiode characteristics of TiO: NiO composite thin structures. *JOURNAL OF MATERIALS AND ELECTRONIC DEVICES, 2*(1).

Demirezen, S., Al-Sehemi, A. G., Yüzer, A., Ince, M., Dere, A., Al-Ghamdi, A. A., & Yakuphanoglu, F. (2022). Electrical characteristics and photosensing properties of Al/symmetrical CuPc/p-Si photodiodes. *Journal of Materials Science: Materials in Electronics, 33*(26), 21011-21021. doi:10.1007/s10854-022-08906-2

Diso, D., Fauzi, F., Echendu, O., Weerasinghe, A., & Dharmadasa, I. (2011). *Electrodeposition and characterisation of ZnTe layers for application in CdTe based multi-layer graded bandgap solar cells.* Paper presented at the Journal of Physics: Conference Series.

Güllü, Ö., Aydoğan, Ş., & Türüt, A. (2012). High barrier Schottky diode with organic interlayer. *Solid State Communications, 152*(5), 381-385.

Hu, X., Zhang, X., Liang, L., Bao, J., Li, S., Yang, W., & Xie, Y. (2014). High-performance flexible broadband photodetector based on organolead halide perovskite. *Advanced Functional Materials, 24*(46), 7373-7380.

Huang, C.-Y., Lin, G.-C., Wu, Y.-J., Lin, T.-Y., Yang, Y.-J., & Chen, Y.-F. (2011). Efficient light harvesting by well-aligned In2O3 nanopushpins as antireflection layer on Si solar cells. *The Journal of Physical Chemistry C, 115*(26), 13083-13087.

İlhan, M., Gorunmez Gungor, Z., Koc, M. M., Coşkun, B., & Yakuphanoğlu, F. (2023). Infrared light sensing performance of CdO-doped TiO2 thin films. *Journal of Materials Science: Materials in Electronics, 34*(1), 67. doi:10.1007/s10854-022-09411-2

Islam, S., Mishra, J. K., Kumar, A., Chatterjee, D., Ravishankar, N., & Ghosh, A. (2019). Ultra-sensitive graphene–bismuth telluride nano-wire hybrids for infrared detection. *Nanoscale, 11*(4), 1579-1586.

Koç, M. M., Dayan, O., Dere, A., Çetinkaya, B., Coşkun, B., & Yakuphanoğlu, F. (2024). A light-detecting Ru(II)/Si heterojunction system involving a binuclear Ru (II) complex with pyridine-2,6-diimine (pydim) ligand. *Journal of Materials Science: Materials in Electronics, 35*(17), 1121. doi:10.1007/s10854-024-12885-x

Kumarage, W. G. C., Wijesundera, R. P., Seneviratne, V. A., Jayalath, C. P., & Dassanayake, B. S. (2017). A study on the enhancement of opto-electronic properties of CdS thin films: seed-assisted fabrication. *Semiconductor Science and Technology, 32*(4), 045014. doi:10.1088/1361-6641/aa5ee3

Kurt, M. S., Aktas, S., Ünal, F., & Kabaer, M. (2022). Optical and Electrical Characterization of a ZnO/Coronene-Based Hybrid Heterojunction Photodiode. *Journal of Electronic Materials*. doi:10.1007/s11664-022-09910-2

Lade, S., & Lokhande, C. (1997). Electrodeposition of CdS from non-aqueous bath. *Materials Chemistry and Physics, 49*(2), 160-163.

Norde, H. (1979). A modified forward I-V plot for Schottky diodes with high series resistance. *Journal of Applied Physics, 50*(7), 5052-5053. doi:10.1063/1.325607

Novoselov, K. S., Geim, A. K., Morozov, S. V., Jiang, D.-e., Zhang, Y., Dubonos, S. V., . . . Firsov, A. A. (2004). Electric field effect in atomically thin carbon films. *Science, 306*(5696), 666-669.

Racko, J., Grmanová, A., & Breza, J. (1996). Extended thermionic emission-diffusion theory of charge transport through a Schottky diode. *Solid-State Electronics, 39*(3), 391-397.

Unal, F., Aktas, S., Kurt, M. S., Koc, M. M., Coskun, B., Aslan, N., . . . Gur, M. (2024). Photodetector performance analysis of a hybrid MnPc/DLC device with high photoresponsivity, sensitivity, and On/Off ratio. *Physica B: Condensed Matter, 695*, 416584. doi:https://doi.org/10.1016/j.physb.2024.416584

Ünal, F. (2013). *InSe ince filmlerinin farklı alt tabanlar üzerinde büyütülmesi ve optik, yapısal, fotoelektrik özelliklerinin araştırılması.* Fen Bilimleri Enstitüsü,

ÜNAL, F. (2021). Investigation Of Some Optical And Electrical Properties Of InSe Thin Film, a Window Layer for Photovoltaic Cell Growth on Glass/GaSe Substrate by M-CBD Method. *Karadeniz Fen Bilimleri Dergisi, 11*(1), 297-306.

Ünal, F. (2022). Investigation of Diode Parameters of Photoconductive and Photovoltaic p-Type Si/Ge-Doped WOx Heterojunction. *Journal of Electronic Materials, 51*(11), 6397-6409. doi:10.1007/s11664-022-09874-3

Wang, J., Fang, H., Wang, X., Chen, X., Lu, W., & Hu, W. (2017). Recent progress on localized field enhanced two-dimensional material photodetectors from ultraviolet—visible to infrared. *Small, 13*(35), 1700894.

Yadav, A. A., & Salunke, S. (2015). Photoelectrochemical properties of In2Se3 thin films: Effect of substrate temperature. *Journal of Alloys and Compounds, 640*, 534-539.

Yan, Y., Abbas, G., Li, F., Li, Y., Zheng, B., Wang, H., & Liu, F. (2022). Self-Driven High Performance Broadband Photodetector Based on SnSe/InSe van der Waals Heterojunction. *Advanced Materials Interfaces, 9*(12), 2102068. doi:https://doi.org/10.1002/admi.202102068

Zhai, T., Ma, Y., Li, L., Fang, X., Liao, M., Koide, Y., . . . Golberg, D. (2010). Morphology-tunable In2Se3 nanostructures with enhanced electrical and photoelectrical performances via sulfur doping. *Journal of Materials Chemistry, 20*(32), 6630-6637.

Zheng, D., Wang, J., Hu, W., Liao, L., Fang, H., Guo, N., . . . Fan, Z. (2016). When nanowires meet ultrahigh ferroelectric field–high-performance full-depleted nanowire photodetectors. *Nano Letters, 16*(4), 2548-2555.